AUTOMATIC ASSESSMENT OF DEVELOPMENTAL DYSPLASIA OF THE HIP

Niamul Quader[1], Antony Hodgson[2], Kishore Mulpuri[3], Thomas Savage[4], Rafeef Abugharbieh[1]

[1]Biomedical Signal and Image Computing Lab- Department of Electrical and Computer Engineering,
[2]Department of Mechanical Engineering, University of British Columbia, Canada.
[3]Pediatric Orthopedics, [4]Pediatric Radiology, British Columbia Children's Hospital, Canada.

ABSTRACT

Developmental dysplasia of the hip (DDH) refers to a spectrum of hip joint abnormalities that may lead to significant adverse consequences if not detected and treated early in infancy. Clinical exam with selective ultrasound (US) imaging is the current standard used for early detection and diagnosis of DDH in infants up to 6 months of age. However, current US systems require specialized training and have considerable between-center variability, which raises concerns of missed early diagnoses and subsequent complications from late treatment. We propose a novel, automatic, and near real-time image analysis approach that extracts bone contours in US images of the neonatal hip and calculates image based dysplasia metrics (alpha and beta angles). We present quantitative validation on 54 US scans of femoral head flexion collected from 10 infants under age of 3 months.

Index Terms— Ultrasound, dynamic dysplasia of the hip, bone imaging, alpha angle, beta angle.

1. INTRODUCTION

DDH is the most common disorder affecting the hip in children, with 1-3% of all newborns diagnosed at birth [1]. This condition refers to a spectrum of defects, ranging from mild dysplasia to total dislocation of the hip, which may lead to significant consequences if not detected and treated early [1, 2]. Although the costs related to DDH screening are relatively modest on a per-infant basis (~$50/infant) [3], since nearly 5M (million) infants are born annually in North America, saving even $10/child in screening costs could have an impact on the order of $50M annually. However, a greater concern is related to the false negatives during early diagnoses as many of these cases often progress to early arthritis while the patients are still adolescents or young adults. When DDH is identified at that point, expensive surgery is the main corrective option. For example, Hoaglund et. al [4] performed a meta-analysis study resulting in a conservative estimate that DDH is the reason behind 10% of adult hip arthroplasties. Nakamura et. al [5] determined that 88% of 2000 consecutive osteoarthritis patients in Japan had DDH. Even taking Hoaglund's conservative estimates, Price et. al [6] noted that approximately 25,000 hip replacement procedures are done annually in the United States alone due to DDH. At approximately $25,000 per procedure, the direct financial impact of these missed early diagnoses is on the order of $600M/year, not including the costs of multiple more expensive revision surgeries later in life or other impacts on the patients' lives.

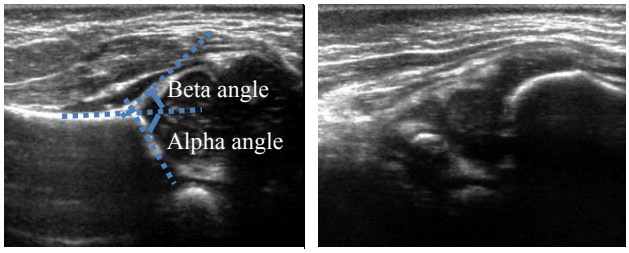

Fig. 1. Example coronal femoral head flexion US images. (a) Adequate US image for dysplasia metric measurements and corresponding alpha and beta angle measurements, (b) Inadequate US image for dysplasia metric measurements.

Ultrasound (US) has been widely accepted as a method for DDH screening in infants. Originally popularized by Graf in the 1980's, US is a non-invasive, non-ionizing, low cost and portable imaging modality for screening [2]. However, a number of studies have raised concern over the efficacy of US in early diagnosis and its economic feasibility in universal screening programs [7, 8]. With high false-positive rates and considerable between-center variability, countries such as Canada and the United States have been hesitant to join European countries in adopting universal ultrasound screening. The between-center variability arises from two major challenges: capturing an adequate US image, and evaluating the dysplasia metrics (see Fig. 1).

Automatic recognition of adequate images and subsequent calculation of key DDH metrics (specifically, alpha and beta angles) could potentially reduce operator skill dependence, improve between-center reliability, and significantly reduce costs. The most important dysplasia metrics are the alpha and beta angles, which are formed from the vertical cortex of the ilium to the acetabular roof and the triangular labral fibrocartilage, respectively (see Fig. 1). To determine these angles, the first step involves extracting the

bone boundaries from the US image. This is particularly challenging because US images are typically characterized by high levels of speckle noise, reverberation, anisotropy, and signal dropout, thereby making it difficult to interpret the image and to reliably detect relevant features [9]. Hacihaliloglu et. al [10] have recently used directional phase symmetry to extract the ridge-like features of bone boundaries in US. A ridge feature is also characteristic of cartilage boundaries and soft-tissue interfaces. However, to effectively extract the complex rounded bone geometries pertaining to DDH assessment, isotropic phase symmetry is needed. We thus propose a novel feature extraction method based on the monogenic signal [11] where we construct a new ridgeness measure that we call the structured phase symmetry (SPS). We demonstrate how this isotropic measure can be effectively used for extracting continuous boundaries and tissue interfaces in neonatal hip images. To the best of our knowledge, our work is the first on automatic US assessment of DDH.

2. METHOD

Given a 2D B-mode US image, $I_{x,y}$, we start by extracting our structured phase symmetry measure, $SPS_{x,y}$ (Section 2.1). To isolate bone boundaries from the $SPS_{x,y}$ responses, we analyze signal attenuation and associated shadowing derived from an US transmission model (Section 2.2). Finally, we determine the presence or absence of the ilium in the US image, and, if present, subsequently determine both the alpha and beta angles (Section 2.3).

2.1. Structured phase symmetry

Bone boundaries and cartilage boundaries can be effectively captured by phase symmetry responses in US images since the beam reflection is significantly weaker both before and beyond these structures where the primary reflection occurs. Phase symmetry can be calculated from the even and odd responses of band-pass quadrature filters as in [10]. Since the desired segmentation is of complex rounded structures, we use the monogenic signal [11] to generate our band-pass quadrature filters. In calculating the monogenic signal, we use the Riesz transform [11], a multidimensional extension of the Hilbert transform.

For the image $I_{x,y}$, the Riesz transform or the odd symmetric response is given by:

$$I_R(x,y) = \begin{pmatrix} I_1(x,y) \\ I_2(x,y) \end{pmatrix} = \begin{pmatrix} h_1(x,y) * I(x,y) \\ h_2(x,y) * I(x,y) \end{pmatrix} \quad (1)$$

where h_1 and h_2 are characterized by the 2D frequency responses $H_1(w) = -jw_x/\|w\|$ and $H_2(w) = -jw_y/\|w\|$ with $w = (w_x, w_y)$. The resulting phase symmetry response can be expressed as:

$$PS(x,y) = \frac{\sum_n |I_n| - |I_{R,n}|}{\sum_n \sqrt{I_n^2 + I_{R,n}^2} + \varepsilon} \quad (2)$$

where ε is a small number to prevent division by zero and n represents the scales of a band-pass filter bank. The band-pass filter bank extracts phase symmetry responses at different scales. We use a log-Gabor filter with a transfer function of $G(w) = \exp(-\log^2\left(\frac{w}{k}\right)/2\log^2(\sigma_w))$, where k is the center frequency of the filter and σ_w controls the bandwidth of the filter [10].

The monogenic signal based isotropic phase symmetry response, $PS(x,y)$, however, remains sensitive to noise and is not able to extract continuous structures. To extract continuous structures, we exploit the near-constant acoustic property of bone, namely that the phase symmetry response along the bone boundaries is nearly constant, resulting in a vessel-like characteristic of bone surfaces in $PS(x,y)$. We quantify this property using a multi-scale vessel-ness measure on PS, inspired by multi-scale vessel-enhancement filtering [12]. Specifically, the second order derivatives of $PS(x,y)$ provide information as to which type of structure the pixel belongs (e.g., a vessel, a blob, an isolated point, etc.). This classification is based on an eigenanalysis of the computed Hessian matrix at each pixel of $PS(x,y)$. The Hessian matrix is computed by convolving $PS(x,y)$ with the second order derivatives of the Gaussian filter bank $G(x,s) = 1/2\pi s^2 \exp(-\|x\|^2/2s^2)$, where s represents the scales of the multi-scale Gaussian filter bank (empirically selected as 2 and 4). We define SPS as:

$$SPS(x,y) = \begin{cases} 0 & if\ \lambda_2 > 0 \\ 1 - \mathrm{e}^{\left(-\frac{|\lambda_1|}{|\lambda_2|}\right)} - \mathrm{e}^{(-Q)} & otherwise \end{cases} \quad (3)$$

where λ_1 and λ_2 are eigenvectors such that $|\lambda_2| \leq |\lambda_1|$, and $Q = \lambda_1^2 + \lambda_2^2$. Also, speckles rarely appear as ridges; thus, we inherently reduce the influence of speckle noise by extracting only the ridge-like structures.

2.2. Ultrasound transmission model

To segment bone boundaries from the $SPS(x,y)$ responses, we make use of the property that the US signal attenuation is high at bone surfaces. To incorporate this attenuation-within our feature, we estimate a US transmission model through a confidence map [13], $m(x,y)$, ranging from 0 to 1, where 0 corresponds to zero signal strength and 1 corresponds to the signal strength generated by the transducer. We then estimate the signal strength at a pixel as the probability of a random walk [14] starting from the pixel reaching the virtual transducer. This is computed from the graph Laplacian matrix which is defined as:

$$L_{ij} = \begin{cases} d_i & if\ i = j \\ -w_{ij} & if\ i\ adjacent\ to\ j \\ 0 & otherwise \end{cases} \quad (4)$$

where $d_i = \sum_j w_{ij}$. The edge weights, w_{ij}, are then assigned in the horizontal, vertical and diagonal directions: $w_{ij}^H = \exp(-\beta(|c_i - c_j| + \gamma))$, and $w_{ij}^V = \exp(-\beta(|c_i - c_j|))$, $w_{ij}^D = \exp(-\beta(|c_i - c_j|))$. The term, c_i, is the depth-based intensity gradient controlled by a parameter α, and γ repre-

sents the penalty of a horizontal and diagonal walk compared to a vertical walk. β controls robustness of the overall result of random walk.

We use the resulting probability, $m(x,y)$, of the above random walk to calculate two features [15]: an attenuation feature $A(x,y) = m_{x,y} - (m_{min})$, and a shadowing feature $S = m_{x,y}/(m_{min})$, where m_{min} is the minimum node value in a $(p \times p)$ window centered around (x,y). Similar to [15], we define a bone membership as:

$$P_{x,y} = \begin{cases} A_{x,y} + S_{x,y} + SPS_{x,y} & if\ SPS > 0 \\ 0 & if\ SPS = 0 \end{cases} \quad (5)$$

We use coordinates (x_m, y_m), corresponding to maximums of $P_{x,y}$ along each scan-line, to evaluate the mean, μ, and the standard deviation, σ, of the confidence map values $m(x_m, y_m)$, and define the probability-based segmentation of bone boundary as:

$$CPS_{x,y} = \begin{cases} P_{x,y} \times SPS_{x,y} & if\ |m_{x,y} - \mu| < \sigma, P_{x,y} > .5 \\ 0 & otherwise \end{cases} \quad (6)$$

2.3. Dysplasia metrics extraction

The commonly used dysplasia metrics are the alpha and beta angles. The alpha angle is formed by the acetabular roof and the vertical cortex of the ilium. The beta angle is formed by the vertical cortex of the ilium and the triangular labral fibrocartilage. To assess whether a scanned US image is adequate for use in extracting dysplasia measurements, we use the criterion that the ilium should be placed parallel to the ultrasound transducer. To do so, we identify the segmented bone boundaries that have minor eigenvectors λ_2 within $\pm 10°$ (set empirically) of any lines parallel to US transducer. We then pare down this set of identified bone boundaries into single pixel strands using a morphological thinning operation, extract the longest line (see Fig. 2), and check whether the length of this line, l, is sufficiently long using the criteria $(l_{max}/2) > l > (l_{max}/6)$, where l_{max} is the width of the B-mode US image. This threshold has been chosen empirically through analyzing a set of pilot images.

Next, we identify the edge of the ilium, (x_1, y_1), closest to the center scan-line $l_{max}/2$. We perform Radon transform of three regions of interest (ROI) around (x_1, y_1): a 30x30 pixel ROI towards the acetabular roof, a 30x30 pixel ROI towards the vertical cortex of the ilium, and a 30x30 pixel ROI towards the triangular labral fibrocartilage (see Fig. 2); thus, all three ROIs are automatically selected based on the location of $(x_1,\ y_1)$. Maximum responses of these Radon transforms correspond to the angles associated with the most dominant structures, i.e., the acetabular roof, vertical cortex of the ilium, and triangular labral fibrocartilage. Thus, the first two ROIs produce the alpha angle, whereas the second and third produce the beta angle. Finally, $alpha = R_2 - R_1$, and $beta = R_3 - R_2$, where R_1, R_2, and R_3 are the peaks in the Radon transforms.

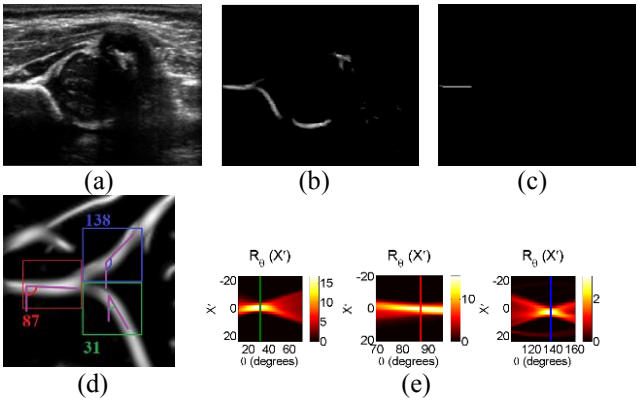

Fig. 2. Extraction of Dysplasia metrics. (a) Example B-mode US image, (b) bone boundary detected as described in Section 2.1 and 2.2, (c) pared down horizontal ilium, (d) SPS with the ROIs for angle calculation as described in Section 2.3, (e) the Radon transforms of ROIs. As seen in (d), $R_1 = 31$, $R_2 = 87$, and $R_3 = 138$. Thus, $alpha = 87 - 31 = 56\ degree$, and $beta = 138 - 87 = 51\ degree$.

3. RESULTS

To validate the performance of our proposed SPS feature, we compared it with two other PS methods (see Fig. 3), based on the monogenic filter [11] and another based on directional filters [10]. Note how the monogenic filter based PS has higher number of false negatives, and how the directional filters based PS tend to straighten the curved boundaries and connect acetabular roof to triradiate cartilage, whereas SPS seem to extract most of the symmetry points accurately, particularly symmetry points at the labrum, ilium, acetabular roof, and triradiate cartilage.

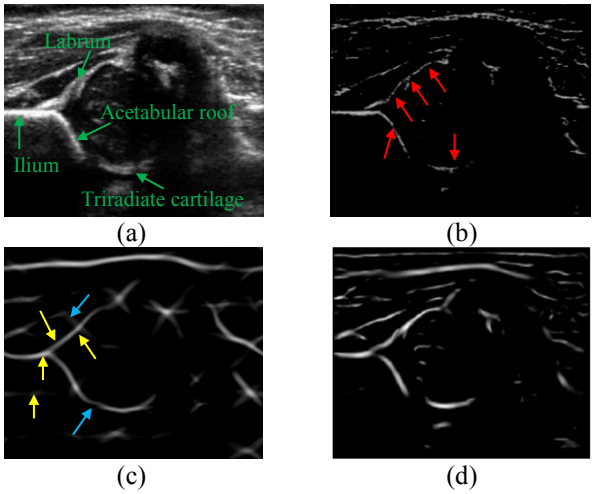

Fig.3. Example qualitative results. (a) B-mode US image of the femoral head, (b) monogenic signal based PS, (c) directional filter based PS, (d) SPS. Red arrows point to false negatives, and yellow arrows point to falsely straightened structures, on the labrum, ilium, acetabulum, and triradiate cartilage. Blue arrows point to falsely connected structures.

Table. 1. Absolute differences between the alpha and the beta angles as derived by our automatic method vs. manually by a radiologist. The absolute differences are well under the differences in the alpha and beta angles between normal and DDH-positive patients, which is typically between 11° and 18°, respectively.

Dysplasia metric	Mean	Standard deviation
Alpha angle	0.61°	0.41°
Beta angle	0.70°	0.58°

To quantitatively evaluate the performance of our proposed automatic assessment of DDH, we validated on 54 B-mode US images collected from 10 infants under 3 months of age (obtained with the appropriate institutional review board approvals in place). First, we compared the automatic selection of adequate US images against manual rankings by an experienced radiologist. Our proposed method failed to select two (out of 33) images judged adequate by the radiologist. All the inadequate images, however, were correctly rejected. This is reassuring since we envision using our system to acquire and process B-mode US images until multiple adequate images are found, thus it is more important to avoid accepting sub-standard images than to occasionally reject an acceptable one (especially since rejected images will likely be borderline images).

Finally, we invited a trained radiologist to make any adjustments he deemed necessary to our automatically extracted alpha and beta angles in the B-mode US images judged to be adequate. The absolute values of the adjustments made by the radiologist are shown in Table 1. The mean absolute difference between manual and automatically-calculated angles is approximately 0.6 degrees for both the alpha and beta angles.

For an adequate B-mode US image, the whole process of image selection and angle extraction took an average of 0.6s. All tests were run using MATLAB on a Xeon(R) 3.40 GHz CPU computer with 8GB RAM.

4. CONCLUSIONS

We proposed a novel automatic approach for assessment of DDH metrics that incorporates both automatic detection of US image adequacy as well as extraction of the alpha and beta angles. To do so, we proposed a novel PS based image feature that incorporates the near-constant acoustic property of bone and cartilage structures. Our tests on pilot clinical data suggest that the extracted alpha and beta angles appear to be reliably close to manually estimated values with a mean difference of $< 1°$. This difference is significantly lower than the difference in the alpha and beta angles between normal and DDH-positive patients, which is typically between 11° and 18°, respectively. The proposed method could potentially reduce operator skill dependence, improve between-center reliability, and significantly reduce costs. Further, the proposed method runs in near real-time hence it promises to be a practical solution in real clinical screening settings. Our future work will focus on real-time implementation of our algorithm on an ultrasound machine, such that it can extract DDH metrics on-the-fly as a patient is undergoing a scan.

5. REFERENCES

[1] M.D. Sewell, K. Rosendahl, and D.M. Eastwood, "Clinical review: developmental dysplasia of the hip," *BMJ*, 339:b4454, 2009.

[2] R. Graf, "Fundamentals of sonographic diagnosis of infant hip dysplasia," *J Pediatr Orthop*, 4(6):735-740, 1984.

[3] T. Woodacre, A. Dhadwal, T. Ball, C. Edwards, and P.J. Cox, "The costs of late detection of developmental dysplasia of the hip," *J Child Orthop*, 8(4):325-332, 2014.

[4] F.T. Hoaglund, and L.S. Steinbach, "Primary osteoarthritis of the hip: etiology and epidemiology," *J Am Acad Orthop Surg*, 9(5):320-327, 2001.

[5] S. Nakamura, S. Ninomiya, and T. Nakamura, "Primary osteoarthritis of the hip joint in Japan," *Clin Orthop Relat Res*, (241):190-196, 1989.

[6] C.T. Price, and B.A. Ramo, "Prevention of hip dysplasia in children and adults," *Orthop Clin North Am*, 43(3):269-279, 2012.

[7] J.J. Dias, I.H. Thomas, A.C. Lamont, B.S. Mody, and J.R. Thompson, "The reliability of ultrasonographic assessment of neonatal hips," *J Bone Joint Surg Br*, 75(3):479-482, 1993.

[8] American Academy of Orthopaedic Surgeons, "Detection and nonoperative management of pediatric developmental dysplasia of the hip in infants up to six months of age," http://www.aaos.org/research/guidelines/DDHGuidelineFINAL.pdf, 2014.

[9] J.A. Noble, and D. Boukerroui, "Ultrasound image segmentation: a survey," *IEEE Trans Med Imaging*, 25(8):987-1010, 2006.

[10] I. Hacihaliloglu, P. Guy, A. Hodgson, and R. Abugharbieh, "Volume-specific parameter optimization of 3D local phase features for improved extraction of bone surfaces in ultrasound images," *International Journal of Medical Robotics and Computer Assisted Surgery*, 2014.

[11] M. Felsberg, and G. Sommer, "The monogenic signal," *IEEE Trans Med Imaging*, 49(12):3136-3144, 2001.

[12] A.F. Frangi, W.J. Niessen, K.L. Vincken, and M.A. Viergever, "Multiscale vessel enhancement filtering," *MICCAI*, pp. 1496:130-137, 1998.

[13] A. Karamalis, W. Wein, T. Klein, and N. Navab, "Ultrasound confidence maps using random walks," *Medical Image Analysis*, 16:1101-1112, 2012.

[14] L. Grady, "Random walks for image segmentation," *IEEE Trans Pattern Anal Machine Intell*, 28(11), 2006.

[15] N. Quader, A. Hodgson, and R. Abugharbieh, "Confidence weighted local phase features for robust bone surface segmentation in ultrasound," *MICCAI Workshop on Clinical Image-based Procedures (CLIP)*, pp. 29-36, 2014.